

Experimental and numerical study on pre-peak cyclic shear mechanism of artificial rock joints

Xinrong Liu^{**1}, Yongquan Liu^{1,3a}, Yuming Lu^{1,4a} and Miaomiao Kou^{*2,5}

¹ School of Civil Engineering, Chongqing University, Chongqing 400045, P.R. China

² School of Civil Engineering, Qingdao University of Technology, Qingdao, 266033, China

³ China Construction Underground Space Co., Ltd., Chengdu, 610081, P.R. China

⁴ Chongqing No.7 Construction Engineering Co., Ltd., Chongqing, 400059, P.R. China

⁵ Cooperative Innovation Center of Engineering Construction and Safety in Shandong Blue Economic Zone, Qingdao, 266033, China

(Received June 29, 2017, Revised October 5, 2017, Accepted November 27, 2019)

Abstract. The pre-peak cyclic shear mechanism of two-order asperity degradation of rock joints in the direct shear tests with static constant normal loads (CNL) are investigated using experimental and numerical methods. The laboratory testing rock specimens contains the idealized and regular two-order triangular-shaped asperities, which represent the specific geometrical conditions of natural and irregular waviness and unevenness of rock joint surfaces, in the pre-peak cyclic shear tests. Three different shear failure patterns of two-order triangular-shaped rock joints can be found in the experiments at constant horizontal shear velocity and various static constant normal loads in the direct and pre-peak cyclic shear tests. The discrete element method is adopted to simulate the pre-peak shear failure behaviors of rock joints with two-order triangular-shaped asperities. The rock joint interfaces are simulated using a modified smooth joint model, where microscopic scale slip surfaces are applied at contacts between discrete particles in the upper and lower rock blocks. Comparing the discrete numerical results with the experimental results, the microscopic bond particle model parameters are calibrated. Effects of cyclic shear loading amplitude, static constant normal loads and initial waviness asperity angles on the pre-peak cyclic shear failure behaviors of triangular-shaped rock joints are also numerically investigated.

Keywords: Pre-peak cyclic shear; Two-order asperity degradation; Shear failure modes; DEM; Numerical simulation

1. Introduction

The discontinuous structures, for instance joints, faults and flaws, often occur in the rock masses (Liu *et al.* 2017, Ma *et al.* 2016, 2019a, b, Zhou *et al.* 2019a, b, Kou *et al.* 2020). The surfaces of rock joints are rough at multiple scales. The surface roughness of rock joints in rock masses, which is one of the most critical factors, significantly affects the mechanical properties and behaviors of joints and jointed rocks (Zheng and Qi 2012, Dang *et al.* 2016). The surface roughness of rock joints has important implications for estimating true contact areas and modeling the hydro-mechanical response of joint asperities during contact between wall surfaces (Belem *et al.* 2007). The contact conditions between two rough rock surfaces strongly influence the shear mechanical behaviors, i.e., shear strength, deformation characteristics and shear failure modes (Huang and Yang 2019, Cai *et al.* 2019). The shear mechanical behaviors of rock joints under complicated loading conditions play a vital role in evaluating the stability of underground rock engineering projects, such as tunnels, underground storages and nuclear waste repositories.

In the past decades, several studies on the shear mechanical behaviors of rock joints were carried out by scholars to understand the shear mechanism of rock joints under constant normal load (CNL) conditions (Bandis *et al.* 1981, 1983, Yang *et al.* 2001, Huang *et al.* 2002, Moradian *et al.* 2010, Dang *et al.* 2018, 2019), where the normal load remains unchanged during shearing, and constant normal stiffness (CNS) conditions (Ooi and Carter 1987, Johnston *et al.* 1987, Benmokrane *et al.* 1994, Seidel and Haberfield 2002, Jiang *et al.* 2004, Zhou *et al.* 2016), in which stiffness of the surrounding rock mass is imitated. To study the effect of surface roughness on shear mechanical behaviors of rock joints in shear tests, the surfaces of rock joints can be classified into the natural rock joints, in which the surface morphology is described as a concept of joint roughness coefficient (JRC) (Barton 1973, 1976, Barton and Choubey 1977), and artificial saw-tooth rock joints, where the surface morphology is designed as periodically triangular and sinusoidal shapes (Zhou *et al.* 2016). Moreover, the surface morphology of rock joints can be considered as multiscale asperities, which can be divided into waviness (i.e., primary asperity) and unevenness (i.e., subordinated asperity) (Jafari *et al.* 2003, 2004). Although the shear mechanical behaviors of natural rock joints and artificial rock joints with waviness have been widely studied, effects of multiscale asperities, including waviness and unevenness, at the surface of rock joints on the shear mechanical behaviors require to be deeply investigated.

On the other hand, according to the actual stress field conditions in rock engineering projects, the loading

*Corresponding author, Ph.D., Associate Professor

E-mail: koumiaomiao@qut.edu.cn

**Co-Corresponding author, Ph.D., Professor

E-mail: liuxrong@126.com

^a Ph.D.

conditions to be taken into consideration in the investigation on failure characteristics of rock masses and mechanical behaviors of discontinuities fall into two main categories, i.e., direct and cyclic types. Some scholars have conducted experiments about the direct shear mechanism of natural and artificial rock joints (Moradian *et al.* 2010, 2012, Meng *et al.* 2016, 2018a, b). However, the cyclic loadings are likely to be encountered in different rock structures in geotechnical earthquake engineering (Bagde and Petroš 2005, Liu *et al.* 2017). Cyclic loading can cause shear failure of the joints (e.g. strong earthquakes) or cause some degradation in pre-peak behavior of joints (e.g. weak earthquakes) (Fathi *et al.* 2016, Song *et al.* 2019, 2020). Some experimental studies on the cyclic shear mechanical behaviors of natural rock joints have been carried out, and they found that the shear mechanical behaviors, such as shear failure modes, normal dilations, shear peak and residual strength, are influenced by the cyclic loading parameters, including shear cyclic number, shear cyclic frequency, shear cyclic amplitude, etc (Lee *et al.* 2001, Jafari *et al.* 2003, 2004, Belem *et al.* 2007, Ferrero *et al.* 2010, Mirzaghorbanali *et al.* 2014a, Fathi *et al.* 2016). Although some cyclic shear mechanical of natural rock joints were successfully investigated, the aforementioned experimental studies are mainly concerned on the peak and post-peak cyclic shear loading conditions, which mainly correspond to the strong earthquakes (Mirzaghorbanali *et al.* 2014a, b, Fathi *et al.* 2016 Yang *et al.* 2018). However, the number of experimental studies on the pre-peak cyclic shear mechanism of rock joints in the weak earthquakes is rare (Seidel and Haberfield 2002, Jafari *et al.* 2003, 2004, Fathi *et al.* 2016). In addition, as stated by Jafari *et al.* (2003, 2004), the failure behaviors of unevenness at the surface of rock joints play significant roles in weak earthquakes, where rock joints containing two-order asperities are subjected to the cyclic shear loads at the pre-peak stage. Thus, it is interesting and necessary to study the pre-peak cyclic mechanical behaviors of artificial rock joints with two-order triangular-shaped asperities.

With development of computer techniques, numerical methodology becomes an efficient tool to study failure characteristics of solids under different loading conditions. Numerical simulations are less expensive than experimental tests and can provide physical insights of different solid failure problems, which are difficult to obtain through pure experimental tests due to the limited monitoring technologies. Numerical methodologies can be categorized into two different approaches: continuous approach and discontinuous approach. For the continuous approach, the finite element method with efficient remeshing techniques (Amiri *et al.* 2014, Areias *et al.* 2013, 2017, Nowruzpour Mehrian *et al.* 2013, Mehrian *et al.* 2016), extended finite element method (Moës and Belytschko 2002, Nanthakumar *et al.* 2016, Xie *et al.* 2016) and peridynamics (Nowruzpour *et al.* 2019, Nowruzpour and Reddy 2018, Zhou and Wang 2016, Zhou *et al.* 2018, 2019c, Wang *et al.* 2016, 2017, 2018a, b, c, d, 2019a, b, c, d) are developed to study the fracture mechanics in solids. For the discontinuous approach, the algorithm in bond particle methodology (Potyondy and Cundall 1998, 2004, Fakhimi 2004, PFC2D

2004, Mohammed *et al.* 2015, Sarfarazi and Haeri 2018, Haeri *et al.* 2018a, b, c, d, e), which is suitable to study the failure behaviors of geomaterials and has been widely applied to geotechnical engineering projects (Zhang and Wong 2012, Cao *et al.* 2016, 2018, Kou *et al.* 2019a, b, c), is normally constituted to generate a homogenous assemble of regular-shaped (spherical) or irregular-shaped (clumps) particles. The bond particle methodology is a microscale-based numerical method formulated on the premise of the element state of solid materials at the microscopic level (Cao *et al.* 2016). Compared with finite element method, the bond particle methodology has ability to obtain initiation and propagation of the fracturing processes, which allows an improved appraisal of geomechanical processes at the microscale. In order to simulate the mechanical behaviors of rock joints, a smooth joint model that has been specifically calibrated to represent an unbonded rock joint. (Eshiet and Shen 2014, 2017, Li and Chen 2017, Li *et al.* 2019) The smooth joint contact model (Asadi *et al.* 2012, 2013, Bahaaddini *et al.* 2013, 2014, 2016) is specially adopted to simulate the shear mechanical behaviors of rock joints in the direct and cyclic shear tests.

In this article, a series of direct and pre-peak cyclic shear tests are performed on the artificial sandstone joints with two-order triangular-shaped asperities to investigate the direct and pre-peak cyclic shear mechanisms of rock joints using the experimental and numerical approaches. The two-order triangular-shaped asperities at artificial rock joints can be divided into two different orders, i.e., primary asperity and subordinate asperity, which represent the waviness and unevenness of rock joint surface roughness, respectively. Three different shear failure modes of rock joints can first be observed in the direct shear tests under different static constant normal loads. Then, the pre-peak cyclic shear mechanism of rock joints is investigated under these three different shear failure modes through a series of pre-peak cyclic shear tests. To thoroughly understand the pre-peak cyclic shear failure behaviors and mechanism of rock joints with two-order triangular-shaped asperities, a bond particle methodology with modified smooth joint model, where the micro-scale slip surfaces are applied at contacts between particles of upper and lower rock blocks. The direct shear numerical results are in good agreement with the experimental results in the direct shear tests of rock joints in terms of qualitative and quantitative fields, which illustrate the correctness of microscopic parameters in the bond particle methodology with smooth joint contact model. The experimental observations are reproduced by the bond particle methodology with smooth joint contact model in numerical simulations, which improve the understanding of shear failure characteristics of rock joints in the pre-peak cyclic shear tests. Moreover, the effects of pre-peak cyclic shear amplitudes, static constant normal loads and initial waviness asperity angle on the pre-peak cyclic shear mechanism of artificial rock joints with two-order triangular-shaped asperities are investigated using the bond particle methodology with smooth joint contact model.

This paper is organized as follows: the experimental preparations and facilities are described in Section 2. The

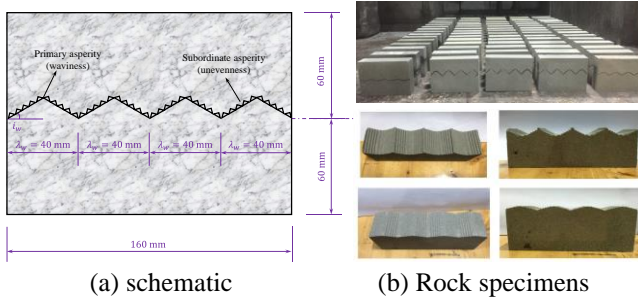


Fig. 1 Geometrical conditions of rock joints in the pre-peak cyclic shear tests

experimental results of rock joints with two-order triangular-shaped asperities under direct and cyclic shear loading conditions are performed in Section 3. The bond particle model and the associated numerical results are stated in Section 4. Discussions about the numerical results are presented in Section 5. Conclusions are drawn in Section 6.

2. Experimental preparations and facilities

2.1 Specimens preparations

In the present study, the rock material is one type of sandstone taken from the Three Gorges Reservoir Region of Chongqing City in China. The average uniaxial compressive strength (UCS) of sandstones is 60.34 MPa respectively, which is measured on the RMT150C testing machine using $\Phi 50 \times 100$ standard cylinder specimens loaded at 0.002 mm/s. The average values of mechanical parameters for Chongqing sandstone are listed as follows: mass density 2,780 kg/m³; Young's modulus 13.63 GPa; Poisson's ratio 0.23; cohesive strength 6.25 MPa; and frictional angle 41.29°. The Chongqing sandstones are first cut into cubic blocks with the dimension 160 mm \times 120 mm \times 60 mm, as shown in Figure 1(a). Then, the cubic specimens are cut into upper and lower blocks based on the designing two-order asperities by the water cutting apparatus, as shown in Fig. 1(a). It can be found from Fig. 1 that the primary and subordinate asperities are triangular-shaped. For the primary asperity, the length of waviness is equal to $\lambda_w = 40$ mm and initial asperity angle equates to i_w , where $i_w = 15^\circ, 30^\circ, 45^\circ$ for three different rock joints. For the subordinate asperity, the initial unevenness angle is kept as a constant, i.e., 45°, and five subordinate triangular-shaped asperities are uniformly distributed at every slope of the primary triangular-shaped asperity, as shown in Fig. 1. To prevent the non-uniform distribution of shear loads in the shear tests, the lateral confinements of jointed sandstone specimens are smoothed and polished. In addition, for sake of investigating the pre-peak shear mechanism of artificial rock joints, a total thirty jointed sandstone specimens are prepared in this study.

2.2 Testing facilities

All the direct and pre-peak cyclic shear tests of the artificial rock joints under static constant normal loads

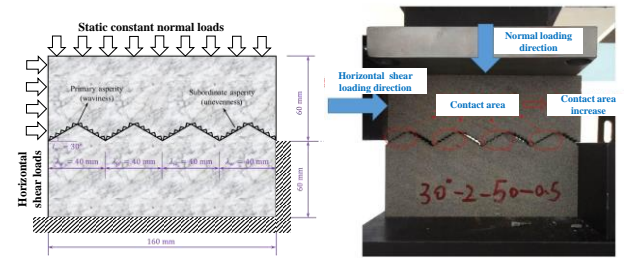


Fig. 2. Loading scheme of the pre-peak cyclic shear tests.

Table 1 Shear testing scheme of artificial rock joints with two-order triangular-shaped asperities

Type	Angle	Stress ^a	Shear Rate ^b	Shear Rate ^c	Amplitud e	N ^d
Direct	15°	1.0				
	15°	2.0	0.5	-	-	-
	15°	4.0				
Cyclic	15°	1.0				
	15°	2.0	0.5	1.0	50%	20-500
	15°	4.0				

^a Normal stress (MPa); ^b Direct shear loading rate (mm/min); ^c Cyclic shear loading rate (mm/min); ^d Shear cyclic number

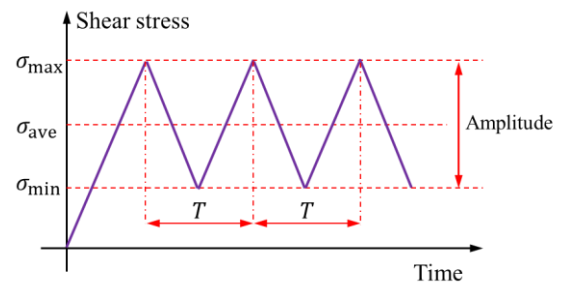


Fig. 3. The pre-peak cyclic shear loading scheme

(CNL) are conducted utilizing the WDAJ-600 type microcomputer controlled electro-hydraulic servorock shear rheological testing machine, as shown in Fig. 2. The maximum normal and shear load capacities for shear tests under CNL conditions of this loading system are 600 kN and 600 kN, respectively. During the present tests, normal loads are applied at a rate of 1 kN/s, and then are held constant. The initial normal loads is vertically applied on the top surfaces of sandstone specimens with artificial two-order triangular-shaped asperities utilizing the hydraulic jack in WDAJ-600 shear rheological machine. The applied normal loads are measured using a calibrated load cell. For the horizontal shear loads, there exist two different loading schemes, including load-controlled scheme and displacement-controlled scheme. The horizontal shear loads are applied using the shear block utilizing hydraulic actuator, as shown in Fig. 2. In the direct and cyclic shear tests, the normal and shear displacements of artificial rock joints are monitored using Linear Variable Differential Transformers (LVDTs) and extensometer.

In the direct shear tests, the displacement-controlled scheme with loading rate of 0.5 mm/min is applied as the horizontal shear loads. In the pre-peak cyclic shear tests, the load-controlled scheme with loading rate of 1.0 kN/s is

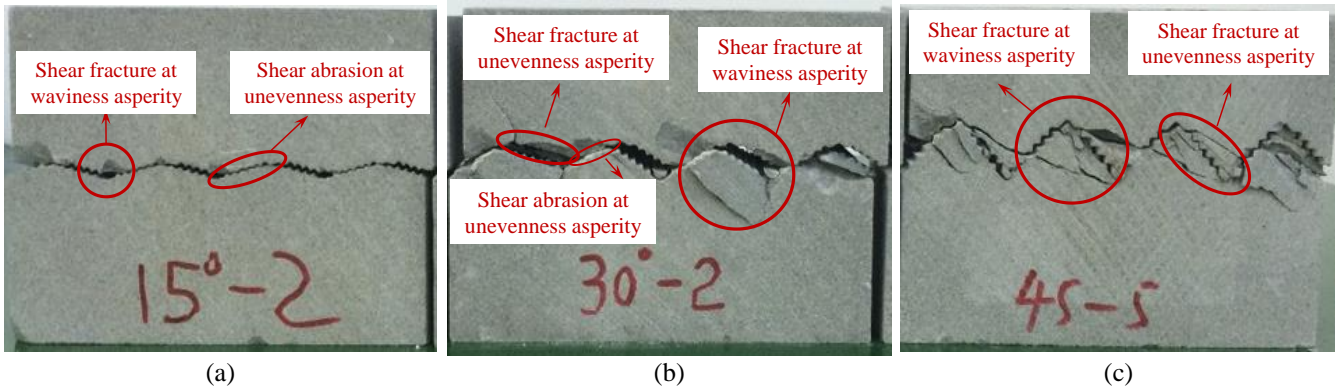


Fig. 4. Three direct shear failure modes: (a) climbing shear failure mode; (b) combined climbing-gnawing shear failure mode; (c) gnawing shear failure mode.

employed to achieve the pre-peak cyclic loads at the pre-peak cyclic loading stage, and the displacement-controlled scheme with rate of 0.5 mm/min are applied. In addition, the maximum shear displacement is set as 10.0 mm in the pre-peak cyclic shear tests.

It should be noted from Fig. 1 and Fig. 2 that the geometrical conditions of the artificial rock joints with two-order triangular-shaped asperities are not symmetrical due to the surface roughness of artificial rock joints. However, the loading conditions, i.e., boundary conditions, applied to the artificial rock joints with two-order triangular-shaped asperities are symmetrical, as shown in Fig. 2.

2.3 Loading scheme

To obtain the direct peak strength and the typical shear failure modes, fifteen tests of the artificial rock joints containing two-order triangular-shaped asperities. In the direct shear tests, three types of artificial rock joints are conducted to determine the peak shear strength and three different typical shear failure modes, i.e., climbing shear failure mode, combined climbing-gnawing shear failure mode, and gnawing shear failure mode, which are commonly observed in the rock slopes and other rock engineering projects (Huang *et al.* 2015, Gu *et al.* 2017), under different static constant normal loads. In addition, to investigate the pre-peak cyclic shear mechanism of artificial rock joints with two-order triangular-shaped asperities for three different direct shear failure modes, fifteen tests are performed for the artificial rock joints under the pre-peak cyclic loading conditions in two consecutive steps. First, load-controlled and then displacement-controlled for the artificial rock joints under the pre-peak cyclic loading conditions. In the load-controlled step, loading cycles with frequency of 0.2 Hz and amplitude of 50% of the peak shear strength of artificial rock joints were applied, as shown in Fig. 3. Pre-peak (i.e., shear load-controlled) cyclic loading shear tests are conducted under different number of shear cycles (20, 50, 100, 200, and 500). The details about direct and pre-peak cyclic shear loading programs of the artificial rock joints with two-order triangular-shaped asperities are listed in Table 1.

3. Experimental results

3.1 Direct shear testing results

To investigate the mechanical behaviors of the artificial rock joints with two-order triangular-shaped asperities, fifteen tests were conducted based on the loading conditions listed in Table 1. Three typical shear failure modes, including climbing shear failure mode, combined climbing-gnawing shear failure mode and gnawing shear failure mode, can be captured in the direct shear tests of the artificial rock joints with two-order triangular-shaped asperities under static constant normal loads.

The three type ultimate shear failure modes of artificial rock joints with two-order asperities in the direct shear tests are performed in Fig. 4. It can be found from Fig. 4(a) that when the initial waviness asperity angle is equal to 15° and the static normal stress equates to 1.0 MPa, the climbing shear failure mode occurs in the direct shear tests. In the climbing shear failure mode, shear abrasion occurs at the unevenness (i.e., subordinate asperities) and shear fracture happens at the waviness (i.e., primary asperities), as shown in Fig. 4(a). When the initial waviness asperity angle is 30° and the static normal stress is 2.0 MPa, the combined climbing-gnawing shear failure mode of the artificial rock joints with two-order triangular-shaped asperities is presented in the direct shear tests, as shown in Fig. 4(b). It can be found from Fig. 4(b) that shear fracture happens not only at the waviness (i.e., primary asperities) but also at the unevenness (i.e., subordinate asperities) in the combined climbing-gnawing shear failure mode. Simultaneously, the shear abrasion also occur at the unevenness (i.e., subordinate asperities) in the combined climbing-gnawing shear failure mode, as shown in Fig. 4(b). When the initial waviness asperity angle is 45° and the static normal stress is 4.0 MPa, the gnawing shear failure mode of the artificial rock joints with two-order triangular-shaped asperities can be observed in the direct shear tests, as shown in Fig. 4(c). The shear fracture occurs at both waviness (i.e., primary asperities) and unevenness (i.e., subordinate asperities) in the gnawing shear failure mode, as shown in Fig. 4(c).

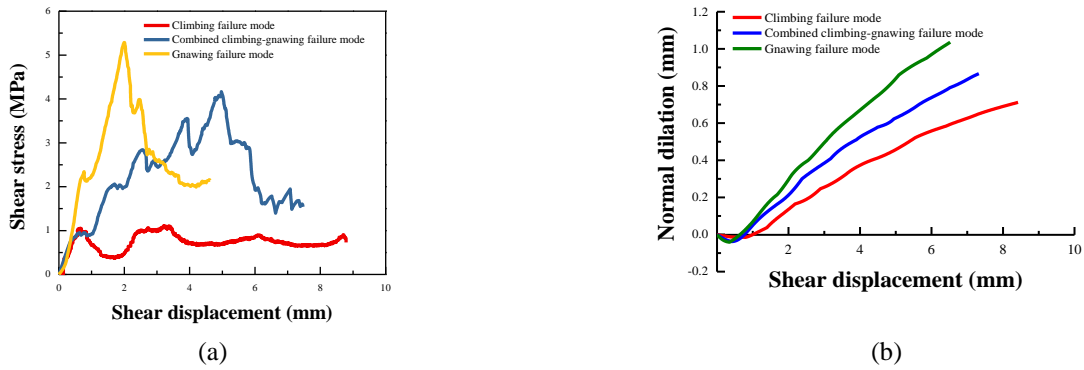


Fig. 5 Mechanical curves for three different direct shear failure modes: (a) shear stress-shear displacement curves and (b) normal dilation-shear

Table 2 Average direct shear strength of rock joints in three shear failure modes

Failure Type	Direct peak shear strength (MPa)					Average (MPa)
I ^a	1.18	0.97	1.05	1.13	1.10	1.09
II ^b	4.23	3.76	3.96	3.68	4.21	3.97
III ^c	5.45	4.92	5.14	5.07	5.22	5.16

^a Climbing failure; ^b Combined climbing-gnawing failure; ^c Gnawing failure

The corresponding typical shear stress versus shear displacement curves of the artificial rock joints with two-order triangular-shaped asperities in the direct shear tests are plotted in Fig. 5(a). Meanwhile, the associated normal dilations curves of rock joints in the shear tests are also presented in Fig. 5(b). It can be found from Fig. 5(a) and Fig. 5(b) that the consolidation of rock joints occurs at the beginning stage of direct shear tests. Then, the degradation and failure of artificial rock joints with two-order triangular-shaped asperities happen with increasing the direct shear displacements, as shown in Fig. 5. The phenomenon of oscillations in the mechanical curves (Fig. 5(a)) can be illustrated by the transition between stick states and slip states of rock joints during direct shearing processes. When the shear failure modes transform from climbing failure mode to gnawing failure mode, more stick states of rock joints occur in the processes of direct shear tests, which demonstrate the less oscillations in the shear stress-displacement curves, as shown in Fig. 5. In addition, the peak shear strength of three different rock joints listed in Table 2. It can be found from Table 2 that the average direct peak shear strength increases when the direct shear failure mode transform from the climbing shear failure mode to the gnawing shear failure mode.

3.2 Pre-peak cyclic shear testing results

To study pre-peak cyclic shear mechanism of artificial rock joints with two-order triangular-shaped asperities, fifteen tests were conducted based on the loading conditions listed in Table 1.

Figure 6(a) shows the shear stress-displacement curves and dilation-shear displacement curves of rock samples containing rock joints with waviness (i.e., primary

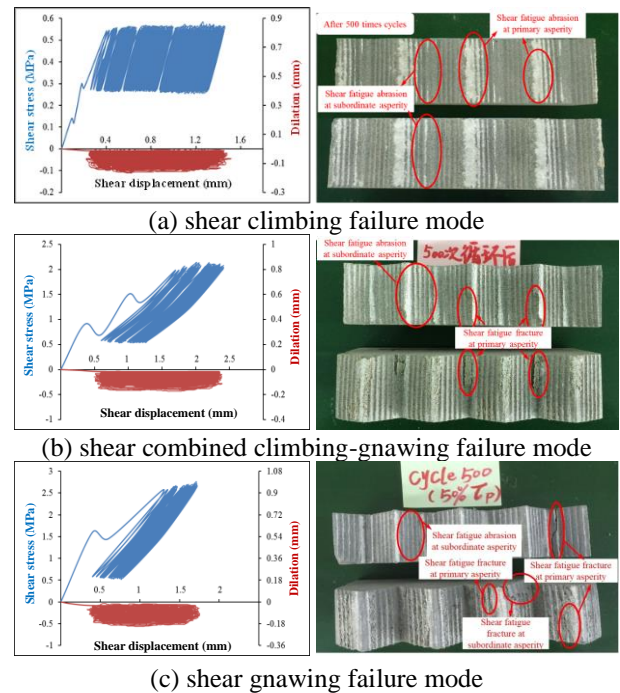


Fig. 6 The pre-peak cyclic shear tests subjected to 500 shear cycles with amplitude of 50% for three different shear failure modes

asperities) inclined at 15° at 500 cyclic shear cycles in the pre-peak cyclic shear loading tests. Figure 6(b) shows the shear stress-displacement curves and dilation-shear displacement curves of rock samples containing rock joints with waviness (i.e., primary asperities) inclined at 30° under at 500 cyclic shear cycles in the pre-peak cyclic shear loading tests. Figure 6(c) shows the shear stress-displacement curves and dilation-shear displacement curves of rock samples containing rock joints with waviness (i.e., primary asperities) inclined at 45° at 500 cyclic shear cycles in the pre-peak shear loading tests. As shown in Figs. 6, the blue solid lines represent the shear strength in the left vertical axes, and the red solid lines are designated as the values of dilation in rock samples in the right vertical axes. The ultimate shear failure modes of rock joints surfaces at the end of pre-peak cyclic shear loading tests are also plotted in Fig. 6.

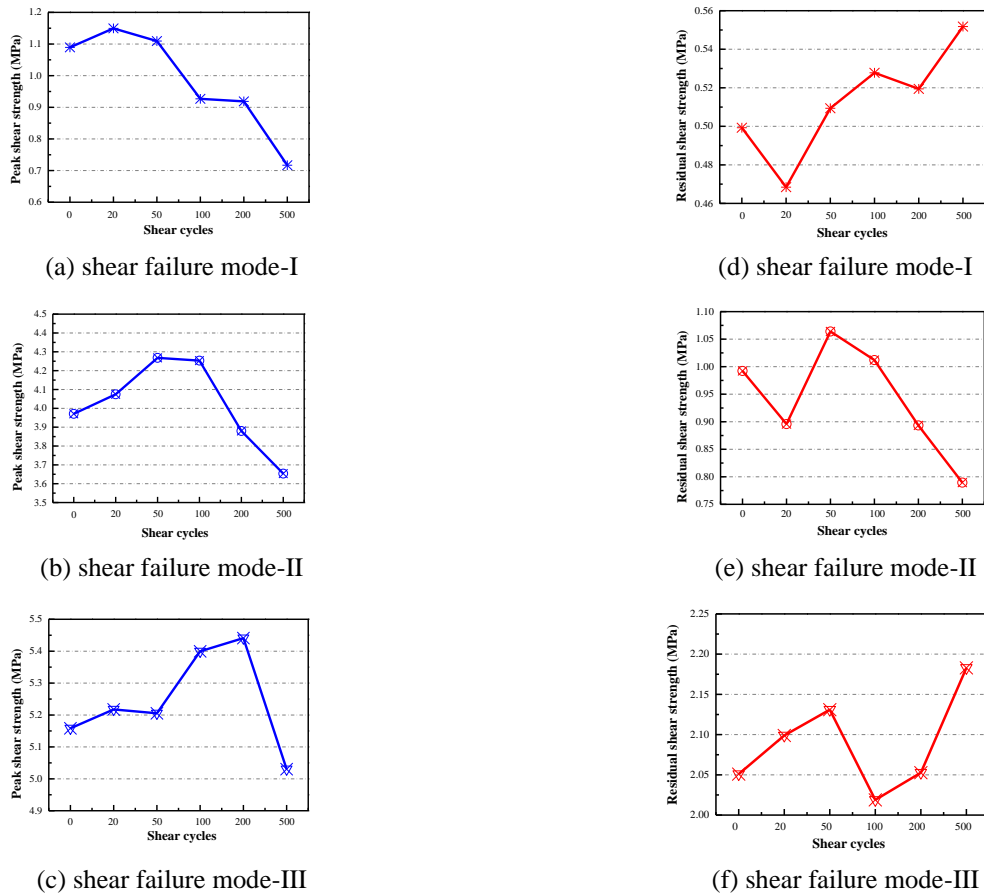


Fig. 7. (a)-(c) Peak and (d)-(f) residual shear strength versus number of pre-peak cycles with amplitude of 50% for three different shear failure modes

When the initial waviness asperity angle of artificial rock joints is equal to 15° the shear abrasion at the unevenness (i.e., subordinate asperities) induces the slight shear stress drop at around 0.2 mm, as shown in Fig. 6(a). It can be found from Fig. 6(a) that once the shear displacement increases to about 0.5 mm, the shear amplitude of 50% of the average maximum direct shear strength reaches. Slightly shear stress drops indicates that the shear fatigue abrasions at the waviness (i.e., primary asperities) and unevenness (i.e., subordinate asperities) maintains the climbing shear failure mode, as shown in Fig. 6(a).

When the initial waviness asperity angle of artificial rock joints is equal to 30° , the mixed climbing-gnawing shear failure mode occurs at the rock joints. It also can be found from Fig. 6(b) that when the shear displacement attains 0.4 mm, drop of shear stress occurs due to the shear abrasions at the unevenness (i.e., subordinate asperities). As the shear displacement increases to about 1.5 mm, the shear amplitude of 50% of the average maximum direct shear strength reaches, as shown in Fig. 6(b). The increasing shear stress drops illustrate that the shear fatigue fracture at the waviness (i.e., primary asperities) and the shear fatigue abrasion at unevenness (i.e., subordinate asperities) both control the shear failure behaviors of the mixed climbing-gnawing shear failure mode of rock joints with two-order triangular-shaped asperities.

When the initial waviness asperity angle of artificial rock joints is equal to 45° , it can be observed from Fig. 6(c) that drop of shear stress occurs due to the shear fatigue fracture at the unevenness (i.e., subordinate asperities) if the shear displacement attains 0.5 mm. As the shear displacement increases to about 1.0 mm, the shear amplitude of 50% of the average maximum direct shear strength reaches, as shown in Fig. 6(c). The intensively shear stress drops indicates the gnawing fracture at the waviness (i.e., primary asperities) controlled the shear failure behaviors of the gnawing failure mode, as shown in Fig. 6(c). It may be caused by the various sequence and degree of contacts between the unevenness (i.e., subordinate asperities) in rock joint.

It can be found from the aforementioned analysis that when the shear failure mode transforms from climbing shear failure mode to gnawing shear failure mode in the pre-peak cyclic shear tests, degradation of the waviness (i.e., primary asperities) and unevenness (i.e., subordinate asperities) changes from shear fatigue abrasion to shear fatigue fracture. Meanwhile, the degree of stress drops becomes larger and the frequency of stress drop becomes higher during the transformation of shear failure modes from climbing shear failure mode to gnawing shear failure mode at the direct loading stage before the application of shear cyclic loads. These phenomena illustrate that the degree of slip states at unevenness (i.e., subordinate

asperities) converts the presence of shear fracture at the pre-peak stage before pre-peak shear cyclic loading conditions.

The effect of pre-peak shear cycles on the peak shear strength and residual peak shear strength are shown in Fig. 7(a)-7(c) and Fig. 7(d)-7(f) in three different shear failure modes of artificial rock joints, respectively.

For the shear failure mode-I (i.e., climbing shear failure mode), the peak shear strength first increases when the pre-peak shear cycles increase from 0 to 20, as shown in Fig. 7(a). Then, Fig. 7(a) shows a clear reduction in the peak shear strength with an increase of pre-peak shear cycle. However, it can be found from Fig. 7(d) that the residual shear strength first decreases as the pre-peak shear cycle changes from 0 to 20. Then, a clear increase of the residual shear strength with increasing the pre-peak shear cycle can be observed from Fig. 7(d).

For the shear failure mode-II (i.e., combined climbing-gnawing shear failure mode), the peak shear strength first increases when the pre-peak shear cycles increase from 0 to 50, as shown in Fig. 7(b). Then, Fig. 7(b) shows a clear reduction in the peak shear strength with an increase of pre-peak shear cycle. However, it can be found from Fig. 7(e) that the residual shear strength first decreases as the pre-peak shear cycle changes from 0 to 20. Then, it can be found from Fig. 7(e) that the residual shear strength of artificial rock joints increases as the pre-peak cycle increases from 20 to 50. Next, a clear reduction of the residual shear strength can be observed after 50 pre-peak shear cycles, as shown in Fig. 7(e).

For the shear failure mode-III (i.e., gnawing shear failure mode), the peak shear strength first increases when the pre-peak shear cycles increase from 0 to 200, as shown in Fig. 7(c). Then, a clear reduction in the peak shear strength with an increase of pre-peak shear cycle, as shown in Fig. 7(c). However, it can be found from Fig. 7(f) that the residual shear strength first increases as the pre-peak shear cycle changes from 0 to 50. Then, it can be found from Fig. 7(f) that the residual shear strength of artificial rock joints decreases as the pre-peak cycle increases from 50 to 100. Next, a clear increase of the residual shear strength can be observed after 100 pre-peak shear cycles, as shown in Fig. 7(f).

Experimental results indicate the shear abrasion of unevenness (i.e., subordinate asperities) leads to the increase of contact area between rock joints under low pre-peak shear cycles in the shear failure modes. The increase of contact area between rock joints result in the increase of shear strengths. With increasing the pre-peak shear cycles, shear fracture at both waviness (i.e., primary asperities) and unevenness (i.e., subordinate asperities) results in the decrease of shear strength.

4. Numerical methods and results

4.1 Bond particle methodology

As an alternative approach based discrete element method, the bond particle methodology (BPM) introduced by Potyondy and Cundall (1998, 2004) show the successful

simulations of rock failure behaviors, including tensile and shear cracks. The major advantage of BPM is that the complex empirical constitutive behavior can be replaced by simple particle contact logic (Zhang and Wong 2012, Huang *et al.* 2016, 2017, 2019). In the framework of bond particle methodology, two basic bond models, namely the contact bond (CB) and the parallel bond (PB) models, are provided to simulate the physical behaviors of solids (Bahaaddini *et al.* 2013). In the previous numerical simulation of shear tests in BPM, the CB model was predominately employed since it reduces the number of micro-parameters compared to the PB model (Park and Song 2009, Asadi *et al.* 2012, 2013). However, it is well understood that the PB model produces a more realistic representation of rock or rock-like materials (Cho *et al.* 2007, Zhang and Wong 2012, Bahaaddini *et al.* 2013, Liu *et al.* 2017). Thus, in the current study, the parallel BPM is utilized to study the pre-peak cyclic shear mechanism of artificial rock joints.

In the parallel bond particle model (PBPM), the intact rock material is represented by a composite of separate particles bonded together. There are two different contact interactions named as normal bonds and tangential bonds based on the deformation characteristics of separate particles. The two different bonds provide the normal and shear stiffness between adjacent interacting particles. In addition, there are two different sets of contact springs bonded among particles. The PBPM approximates the mechanical behaviors of brittle and quasi-brittle connecting the two adjacent particles, which acts like a beam resisting the moment induced by the particle rotation or shearing within the bonded region (Zhang and Wong 2012). According to the remarks by Cho *et al.* (2007), the PBPM is a more realistic bond model for rock-like or rock materials whereby the bonds may break in either tension or shearing with an associated reduction in stiffness (Bahaaddini *et al.* 2013). Based on the previous studies (Zhang and Wong 2012, Huang *et al.* 2015, Bahaaddini *et al.* 2013), the first set of springs between two adjacent particles belongs to grain behaviors providing normal and shear stiffness k_n and k_s , respectively. While, the second set of springs between two adjacent particles belongs to bond behaviors providing the parallel bond normal and shear stiffness \bar{k}_n and \bar{k}_s , which are uniformly distributed over a disc shaped cross section lying on the contact plane.

The normal and shear stiffness representing the grain behaviors between two adjacent particles can be expressed as

$$k_n = 2tE_c \quad (1)$$

$$k_s = \frac{k_n}{k_n/k_s} \quad (2)$$

where $t = 1$ is the thickness for two-dimensional cases, E_c denotes Young's modulus of the particle; k_n/k_s is designated as the ratio of normal to shear stiffness of the particle.

The normal and shear stiffness of parallel bond between two interacting material particles are assigned as

$$\bar{k}_n = \frac{\bar{E}_c}{R^{(A)} + R^{(B)}} \quad (3)$$

$$\bar{k}_s = \frac{\bar{k}_s}{\bar{k}_n/\bar{k}_s} \quad (4)$$

in which \bar{E}_c denotes the Young's modulus of the parallel bond; $R^{(A)}$ and $R^{(B)}$ are the radii of any two neighbouring particles; and \bar{k}_n/\bar{k}_s represents the ratio of normal to shear stiffness of the parallel bond.

The average radius of parallel bond between two interacting adjacent particles is given by

$$\bar{R} = \bar{\lambda} \min(R^{(A)}, R^{(B)}) \quad (5)$$

where $\bar{\lambda}$ is the radius multiplier, which is used to set the parallel bond radius \bar{R} .

A parallel bond between two interacting adjacent particle activates over a finite area and can resist the rotation of particles. The tensile and shear stresses acting on the parallel bond periphery can be calculated from the beam theory. When the maximum tensile stress exceeds the tensile strength of the parallel bond, i.e., $\bar{\sigma}_c$ or the maximum shear stress exceeds the shear strength of the parallel bond, i.e., $\bar{\tau}_c$. Once the parallel bond is broken under shear stress, the shear strength of the parallel bond falls into its residual value. Whereas, when the breakage of a bond occurs induced by the tensile stress, the tensile strength of a parallel bond is set as zero. The residual shear strength is dependent on the normal force and the coefficient of friction of particles, i.e., μ , at the contacts, which can be referred to literatures (Potyondy and Cundall 2004, PFC2D 2004, Zhang and Wong 2012) for details.

4.2 Smooth joint model

The smooth joint model is a developed method for simulation of rock discontinuities in PBPM (Potyondy and Cundall 2004, PFC2D 2004, Cho *et al.* 2007, Bahaaddini *et al.* 2013), which is proposed to simulate the direct shear tests (Bahaaddini *et al.* 2013, 2016). In the smooth joint model, the rectangular slip surfaces are assigned to all contacts between two interacting particles lying on the opposite sides of the joint planes. The joint plane are composed of two coincident planar surface. The orientation of these surfaces is defined by the joint unit normal and tangential vectors, i.e., $\hat{\mathbf{n}}_j$ and $\hat{\mathbf{t}}_j$. The unit normal vector $\hat{\mathbf{n}}_j$ of the joint surface can be described by the joint dip angle θ_p using the following relationships

$$\hat{\mathbf{n}}_j = (\sin \theta_p, \cos \theta_p) \quad (6)$$

The smooth joint is assigned at a contact between particles their centers lying on opposite sides of the joint plane. In order to determine in which surface each particle lies, the dot product of unit normal vector $\hat{\mathbf{n}}_j$ and the contact unit normal vector $\hat{\mathbf{n}}_c$ is used. The contact unit normal vector $\hat{\mathbf{n}}_c$ is along the direction the line connected the centers of two interacting particles. If the $\hat{\mathbf{n}}_j \cdot \hat{\mathbf{n}}_c \geq 0$, the smooth joint lies on the lower surface. The smooth joint is applied in the direction parallel to the joint plane and

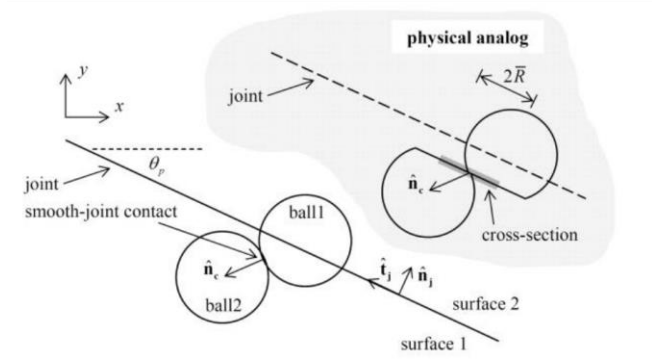


Fig. 8 Illustration of smooth joint contact model in discrete element method (PFC2D 2004)

remains active while there is a nonzero overlap between particles, as shown in Fig. 8.

When we create the smooth joint, the bond connecting two particles is removed and a set of elastic spring is applied uniformly over a rectangular cross section. The area of smooth joint cross section A in a two-dimensional case can be given by

$$A = 2\bar{R}t \quad (7)$$

The force vector \mathbf{F} and the displacement vector \mathbf{U} can be expressed in the local coordinate system of the joint plane. In the local coordinate system of the joint plane, the force and displacement can be expressed as

$$\mathbf{F} = F_n \hat{\mathbf{n}}_j + \mathbf{F}_s \quad (8)$$

$$\mathbf{U} = U_n \hat{\mathbf{n}}_j + \mathbf{U}_s \quad (9)$$

in which F_n is the normal force and U_n is the normal displacement, and \mathbf{F}_s and \mathbf{U}_s denote the shear force and the relative shear displacement vectors, respectively.

It should be noted that the positive values of F_n and U_n respectively represents the compression and overlap. At each time step, the relative displacement increment between two interacting adjacent particles intersected by the smooth joint can be decomposed into normal and tangential components to the joint surface, which can be described as

$$F_n \stackrel{\text{def}}{=} F_n + \bar{k}_{nj} A \Delta U_n^e \quad (10)$$

$$\mathbf{F}_s' \stackrel{\text{def}}{=} \mathbf{F}_s - \bar{k}_{sj} A \Delta \mathbf{U}_s^e \quad (11)$$

The greatest possible value of shear force F_s^* is dependent on the smooth joint coefficient of friction μ_j , which is given by

$$F_s^* = \mu_j F_n \quad (12)$$

At the end of each time step, if $\|\mathbf{F}_s'\| \leq F_s^*$, the $\|\mathbf{F}_s\| = \|\mathbf{F}_s'\|$. Otherwise, the sliding happens at the joint surface, and $\|\mathbf{F}_s\| = F_s^*$.

4.3 Simulation of direct shear tests

In order to calibrate the PBPM micro-parameters, the direct shear tests of artificial rock joints with two-order triangular-shaped asperity with width 160 mm and height

Table 3 Microscopic parameters of the spherical particles and bonds in numerical model

Particle parameters		Parallel bond parameters	
E_c	13.5 GPa	\bar{E}_c	13.5 GPa
k_n/k_s	2.6	\bar{k}_n/\bar{k}_s	2.0
R_{max}	0.51 mm	$\bar{\sigma}_c$	22.5 ± 5 MPa
R_{min}	0.35 mm	$\bar{\tau}_c$	36.5 ± 5 MPa
R_{max}/R_{min}	1.457	$\bar{\lambda}$	1.1
μ	0.5		
ρ	2,700 kg/m ³		

Table 4 Microscopic parameters of smooth joints

Property	k_{nj}	k_{sj}	μ_j	σ_c	c	φ
Value	100 GPa/m	100 GPa/m	0.3	0.0 MPa	0.0 MPa	0

120 mm are generated in the Particle Flow Code (PFC) (PFC2D 2004). The numerical artificial rock joints with two-order triangular-shaped asperities involve the productions of dense packing of non-uniform and well connected spherical particles, and the installation of parallel bonds at contact particles. In the computational domain, there exist 20,316 rock material particles with mass density of 2,700 kg/m³. The maximum and minimum radii (R_{max} and R_{min}) of spherical particles are equal to 0.51 mm and 0.35 mm, respectively, which satisfies a uniform particle-size distribution. The porosity of spherical rock material particles is equal to 0.14 and is uniformly distributed. The smooth joint surfaces are set in the numerical specimen based on the geometrical conditions of artificial rock joints, which separate the rock specimens into upper and lower rock blocks. The microscale parameters in the artificial rock joints with two-order triangular-shaped asperities are listed in Table 3. Moreover, the microscopic parameters of smooth joints are listed in Table 4.

The normal loads is applied vertically to the upper block and this load is kept constant during the numerical tests based on Table 1. The lower blocks are kept stationary during the direct shear tests. The horizontal velocity of 0.2 m/s is applied to the upper rock blocks. The explicit time stepping algorithm is employed in the numerical simulations by PFC. The time step (Δt) in each calculation has small value of $\Delta t = 4.0 \times 10^{-8}$ s, which means that the upper blocks move horizontally at the rate of 4.0×10^{-9} m/time step. The small displacement rate is slow enough to ensure the numerical specimens remains in the quasi-static equilibrium. In the numerical simulations, the shear displacement is measured by tracing the horizontal displacement of the upper block and the shear stress is calculated by dividing the recorded the reaction force on the left wall. In this study, three different artificial rock joints with two-order triangular-shaped asperities are simulated in the PBPM.

Three types of saw tooth-shaped joint profiles with waviness angle i_w of 15°, 30° and 45°, and the same wavelengths $\lambda_w = 40$ mm are numerically simulated. The direct shear tests of the artificial rock joints with initial waviness angles of 15°, 30° and 45° under various constant

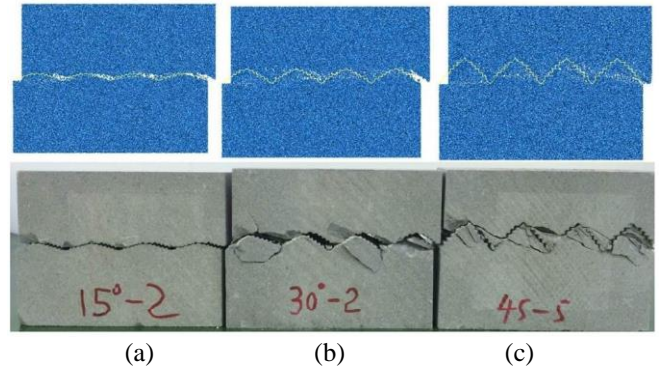


Fig. 9 Comparison of direct shear failure patterns obtained from numerical simulations and experimental observations: (a) climbing shear failure mode, (b) combined shear climbing-gnawing failure mode and (c) gnawing shear failure mode

normal loads, i.e., 1.0 MPa, 2.0 MPa and 4.0 MPa, are simulated using the PBPM. Figure 10 shows three different ultimate shear failure modes for the three types of artificial rock joints with two-order triangular-shaped asperities. The numerical results are in good agreement with the experimental observations, as shown in Fig. 9.

When the static constant normal loads is equal to 1 MPa for the artificial rock joints with initial waviness angles of 15°, the primary asperities remains nearly intact, where the surface roughness slid up the opposite one, thereby resulting in a few cracks of contact, as shown in Fig. 9(a). Meanwhile, the damage and some cracks occur at the subordinate asperities in the direct shear tests, which belongs to the climbing shear failure mode. When the static constant normal loads is equal to 2.0 MPa for the artificial rock joints with initial waviness angles of 30°, some cracks happen at both primary and subordinate asperities in the direct shear tests, which is named as the combined shear climbing-gnawing failure mode, as shown in Fig. 9(b). When the static constant normal loads is equal to 4.0 MPa for the artificial rock joints with initial waviness angles of 45°, several cracks and damage occurs at the both primary and subordinate asperities in the direct shear tests and the phenomenon of failure at the primary asperities can be obtained in the numerical simulations, as shown in Fig. 9(c). The degradation of both primary and subordinate asperities reduces the shear resistance to nearly the residual value. The shear failure mode of the artificial rock joints with initial waviness angles of 45° can be attributed into the gnawing shear failure mode.

The shear stress versus shear displacement graphs for three different types of artificial rock joints with two-order triangular-shaped asperities obtained by the experimental and numerical approaches are shown in Fig. 10. Compared with the experimental data, the present numerical results obtained by the PBPM show good agreement, as shown in Fig. 9. From the qualitative and quantitative analysis of direct shear tests for the artificial rock joints with two-order triangular-shaped asperities, the microscopic parameters in the parallel bond particle model are suitable to simulate the shear tests of artificial rock joints.

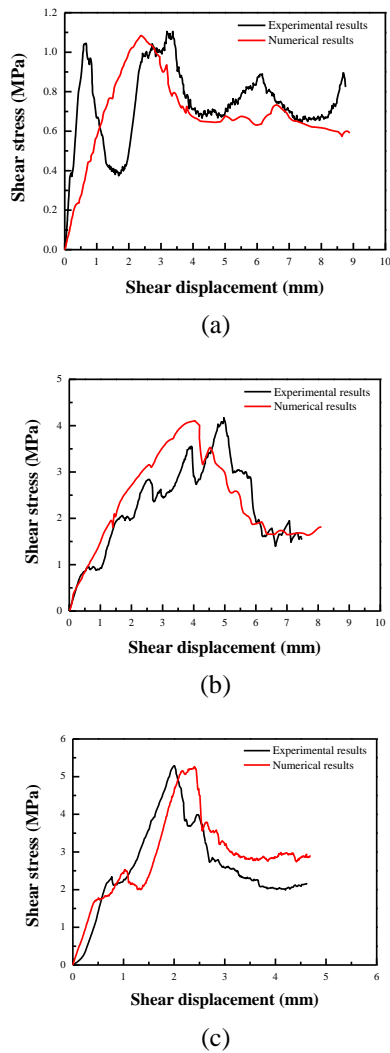


Fig. 10 Comparison of stress-displacement curves for different direct shear tests with different initial waviness asperity angles of (a) 15° , (b) 30° and (c) 45°

4.4 Results for pre-peak cyclic shear tests

To simulate the pre-peak cyclic shear tests of three different types of artificial rock joints with two-order triangular-shaped asperities, two loading schemes are applied in the numerical simulations. For the shear load-controlled loading scheme, the horizontal velocity of 0.2 m/s is applied to the upper rock blocks along the direction from left to right. When the reactive stress on the upper rock blocks is equal to the 50% amplitude of the direct peak shear strength of the artificial rock joints, the horizontal velocity of -0.2 m/s is applied to the upper rock blocks along the direction from right to left. After the shear cyclic number is equal to 500, the direct horizontal velocity of 0.2 m/s is then applied to the upper rock blocks until the shear displacement reaches 10 mm.

For the artificial rock joints with initial waviness asperity angle of 15° in the pre-peak cyclic shear tests, the shear failure processes are presented in Fig. 11. When the pre-peak cyclic number is 20, a few of tensile cracks occurs

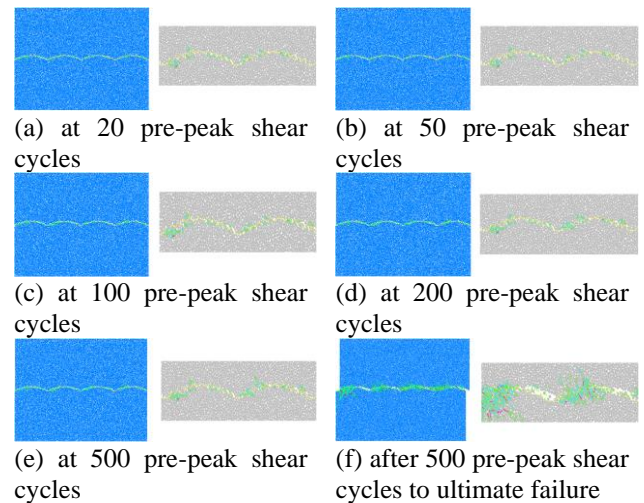


Fig. 11 Shear failure process of rock joints with initial waviness asperity angle of 15° in the pre-peak cyclic shear test with amplitude of 50% (red color represents shear crack and green color represents tensile crack)

at the end of the subordinate asperities and little shear cracks happens at the primary asperities, as shown in Fig. 11(a). When the shear cycle is equal to 50, the number of tensile crack at the subordinate asperities increases, as shown in Fig. 11(b). When the shear cycle increases to 100 times, the number of tensile cracks continues to increase, and some tensile cracks propagate towards the upper and lower blocks, as shown in Fig. 11(c). When the shear cycle is equal to 200 times, some phenomenon of failure occurs at the subordinate asperities induced by the tensile cracks, as shown in Fig. 11(d). When the number of shear cycles is 500 times, the tensile cracks initiated at the subordinate asperities coalesce with other tensile cracks, and the some shear cracks initiated at the end of primary asperities link with the tensile cracks emanating from the subordinate asperities, which leads to the degradation of the primary asperities, as shown in Fig. 11(e). After 500 shear cycle, the climbing shear failure mode are presented in the artificial rock joints with initial waviness angle of 15° under static constant normal loads of 1MPa, as shown in Fig. 11(f). Numerical results mean that the climbing shear failure mode of artificial rock joints is mainly dominated by the tensile microscopic cracks, which belongs to the tensile failure type.

For the artificial rock joints with initial waviness asperity angle of 30° in the pre-peak cyclic shear tests, the shear failure processes are presented in Fig. 12. When the pre-peak cyclic number is 20, some shear and tensile cracks are initiated at the end of subordinate asperities, as shown in Fig. 12(a). When the shear cycle is equal to 50, the number of shear crack at the subordinate asperities increases, and shear cracks initiated at the subordinate asperities coalesce with each other, as shown in Fig. 12(b). When the shear cycle increases to 100 times, the number of shear cracks continues to increase, and some shear cracks propagate towards the upper and lower rock blocks, as shown in Fig. 12(c). Meanwhile, it can be observed from Fig.12(c) that the tensile cracks do not propagate. When the shear cycle is

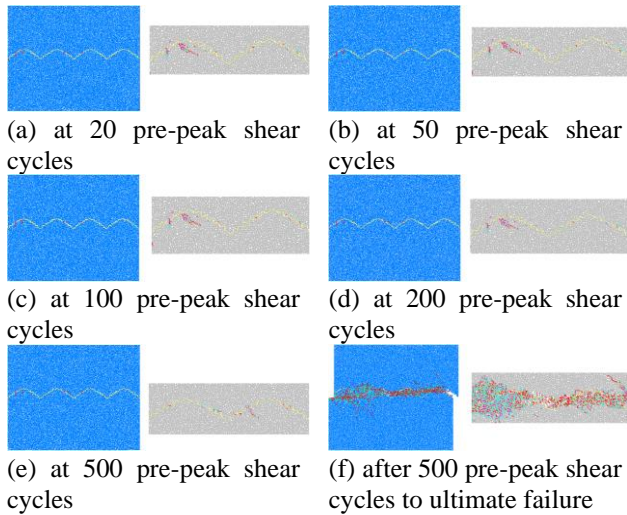


Fig. 12. Shear failure process of rock joints with initial waviness asperity angle of 30° in the pre-peak cyclic shear test with amplitude of 50% (red color represents shear crack and green color represents tensile crack)

equal to 200 times, the shear cracks initiated at the subordinate asperities coalesce with some tensile cracks and some shear cracks at the subordinate asperities, as shown in Fig. 12(d). When the number of shear cycles is 500 times, the crack coalescence of shear cracks and tensile cracks leads to the failure of the primary asperities, as shown in Fig. 12(e). After 500 shear cycle, the climbing shear failure mode are presented in the artificial rock joints with initial waviness angle of 30° under static constant normal loads of 2.0 MPa, as shown in Fig. 12(f). It can be found from Fig. 12(f) that the phenomena of failure at the primary asperities are induced by the shear cracks. Numerical results indicate that the combine climbing-gnawing shear failure mode of artificial rock joints is mainly controlled by coalescences of shear cracks at both the primary and subordinate asperities, which belongs to the combined shear failure type.

For the artificial rock joints with initial waviness asperity angle of 45° in the pre-peak cyclic shear tests, the shear failure processes are presented in Fig. 13. When the pre-peak cyclic number is 20, some shear cracks are initiated at end of the subordinate asperities and some tensile cracks occurs at the primary asperities, which is near the end of the subordinate asperities, as shown in Fig. 13(a). When the shear cycle is equal to 50, the shear cracks initiated at the subordinate asperities coalesce with each other, which leads to the failure of subordinate asperities, as shown in Fig. 13(b). Meanwhile, the tensile cracks emanating from the subordinate asperities propagate towards the upper and lower blocks, as shown in Fig. 13(b). When the shear cycle increases to 100 times, the number of tensile cracks increases, and crack coalescence of shear cracks also increases, as shown in Fig. 13(c). When the shear cycle is equal to 200 times, both tensile and shear cracks initiated at the subordinate asperities propagates towards the upper and lower blocks, as shown in Fig. 13(d). When the number of shear cycles is 500 times, the tensile cracks initiated at the subordinate asperities coalesce with shear cracks initiated at other subordinate asperities, which

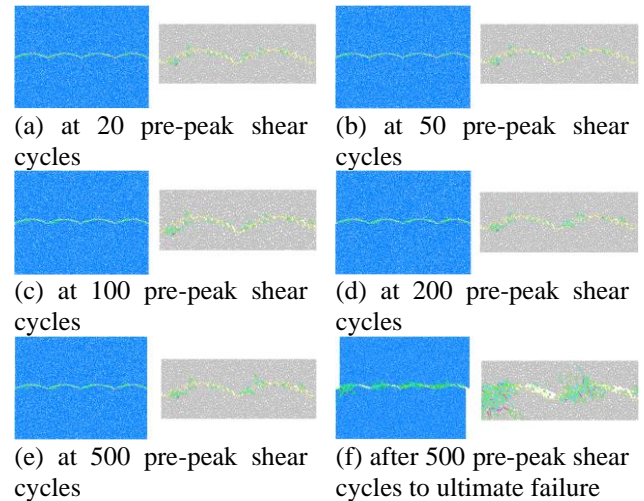


Fig. 13 Shear failure process of rock joints with initial waviness asperity angle of 45° in the pre-peak cyclic shear test with amplitude of 50% (red color represents shear crack and green color represents tensile crack)

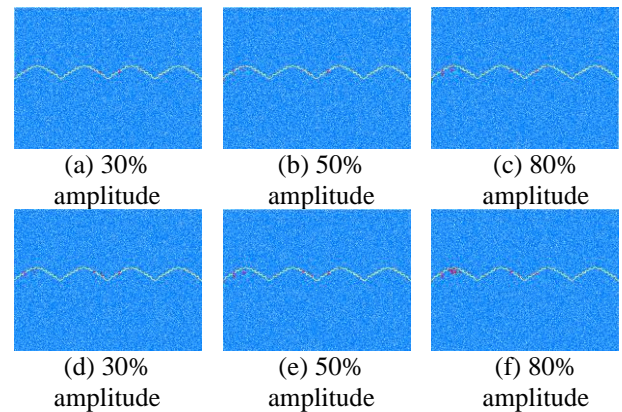


Fig. 14. Pre-peak cyclic shear failure modes of rock joints initial waviness asperity angle of 30° after (a)-(c) 100 shear cycles and (d)-(f) 500 shear cycles with different amplitudes

results in the failure of the primary asperities, as shown in Fig. 13(e). After 500 shear cycle, the climbing shear failure mode are presented in the artificial rock joints with initial waviness angle of 45° under static constant normal loads of 4.0 MPa, as shown in Fig. 13(f). Numerical results demonstrate that the gnawing shear failure mode of artificial rock joints is mainly controlled by coalescences of tensile cracks and shear cracks at both the primary and subordinate asperities, which belongs to the combined tensile-shear failure type.

5. Discussions

5.1 Effect of pre-peak cyclic shear amplitude

To investigate the effect of pre-peak cyclic shear amplitude on the shear mechanical behaviors of artificial rock joints with two-order triangular-shaped asperities, three numerical rock joints with initial waviness angle of

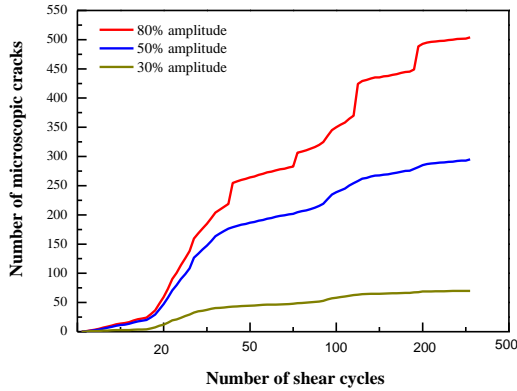


Fig. 15. Microscopic crack evolutions of rock joints containing initial waviness asperity angle of 30° under pre-peak cyclic shear loads with different amplitudes

30° are numerical simulated under the static constant normal loads of 2.0 MPa. The pre-peak cyclic loading amplitudes for three numerical rock joints with initial waviness angle of 30° are employed as 30%, 50% and 80% in the bond particle numerical simulations.

Fig. 14 shows the failure crack patterns of three different numerical rock joints under the pre-peak cyclic shear loading conditions. When the number of shear cycles is equal to 100, some shear cracks occurs at the subordinate asperities in the artificial rock joints under pre-peak cyclic loading amplitude of 30%, as shown in Fig. 14(a). When the pre-peak cyclic loading amplitude increases to 50%, the number of shear cracks initiated at the subordinate asperities increases in the shear cycle of 100 times, as shown in Fig. 14(b). For the pre-peak cyclic loading amplitude of 80%, when the shear cycle equates to 100 times, the number of shear cracks initiated at the subordinate asperities increases and the coalescence of shear cracks occurs at the subordinate asperities, as shown in Fig. 14(c). At the end of 500 times pre-peak shear cycles, it can be found from Fig. 14(d)-Fig. 14(f) that the number of shear cracks initiated at the subordinate asperities increases with increasing the pre-peak cyclic shear amplitude. In addition, it can be found from Fig. 14(e) that the coalescence of shear crack occurs at the subordinate asperities when the pre-peak cyclic shear amplitude is 50% at the end of 500 times pre-peak shear cycles. Simultaneously, crack coalescence induced by the shear cracks at the primary asperities in the numerical artificial rock joints under the pre-peak cyclic shear loading with amplitude of 80% at the end of 500 times pre-peak shear cycles, as shown in Fig. 14(f). Fig. 15 shows the microscopic crack evolutions of rock joints containing initial waviness asperity angle of 30° under pre-peak cyclic shear loads with different amplitude. It can be found from Fig. 15 that the number of microscopic cracks increases as the pre-peak cyclic shear loading amplitude increases during the pre-peak shear cyclic tests.

5.2. Effect of static constant normal loads

To investigate the effect of static constant normal loads on the shear mechanical behaviors of artificial rock joints

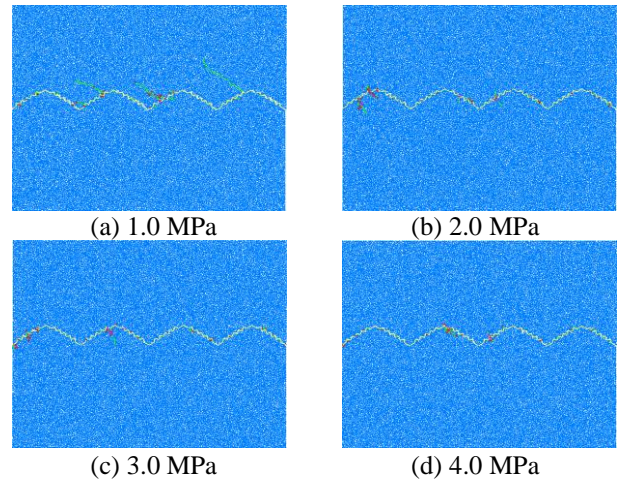


Fig. 16. Pre-peak cyclic shear failure modes of rock joints containing initial waviness asperity angle of 30° after 500 shear cycles with 50% amplitude

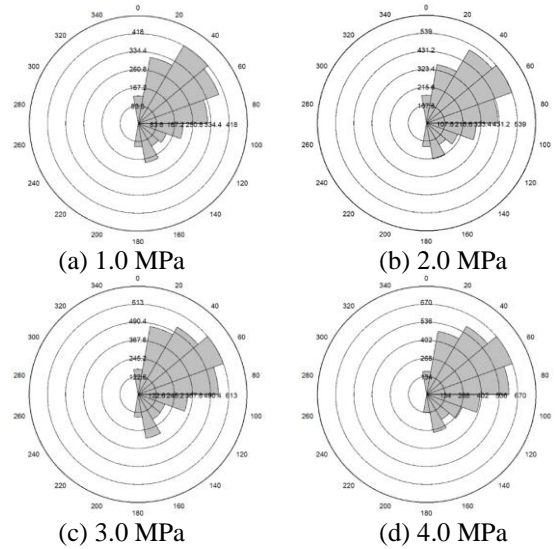


Fig. 17 Discrete fracture network rose diagram of rock joints under different static constant normal loads in the pre-peak cyclic shear tests

with two-order triangular-shaped asperities, four numerical rock joints with initial waviness angle of 30° are numerical simulated under the different static constant normal loads and the same pre-peak cyclic shear loading amplitude of 50%. The static constant normal loads for four numerical rock joints with initial waviness angle of 30° are adopted as 1.0 MPa, 2.0 MPa, 3.0MPa and 4.0 MPa in the bond particle numerical simulations.

Fig. 16 shows four failure patterns of numerical rock joints initial waviness angle of 30° under pre-peak cyclic shear loading amplitude of 50% and different static constant normal loads at the end of 500 time pre-peak shear cycles. It can be found from Fig. 16(a) that some tensile and shear cracks are initiated at the subordinate asperities, and the tensile and shear cracks propagate towards the upper rock blocks in the rock joints under the static constant normal load of 1.0 MPa. When the static constant normal loads increase to 2.0 MPa, the number of shear cracks increases and the number of tensile cracks decreases, as shown in Fig.

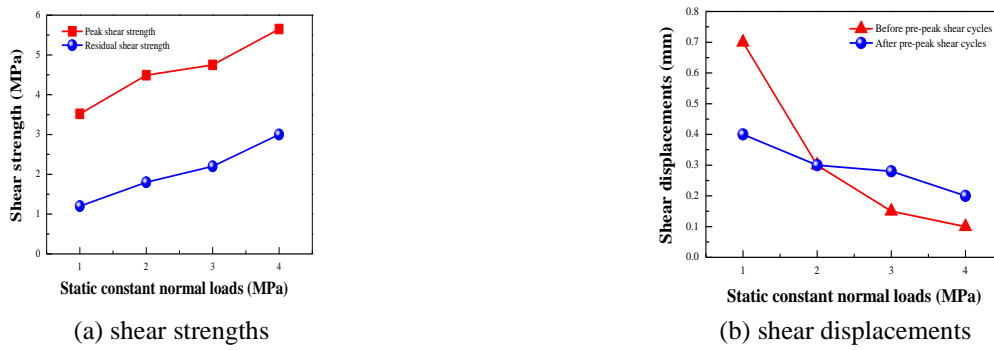


Fig. 18. Effect of static constant normal loads on (a) shear strengths and (b) shear displacements of rock joints after 500 shear cycles in the pre-peak cyclic shear tests

16(b). When the static constant normal load is equal to 3.0 MPa, the number of shear cracks continue to increase, and the number of tensile cracks continue to decrease, as shown in Fig. 16(c). Meanwhile, it can be found from Fig. 16(c) that the coalescence of shear crack occurs at the subordinate asperities as the static constant normal load increases to 3.0 MPa at the end of 500 times pre-peak shear cycle. As the static constant normal load increases to 4.0 MPa, crack coalescence of shear cracks happens not only at the subordinate asperities, but also at the primary asperities, as shown in Fig. 16(d).

Fig. 17 shows the discrete fracture network (DFN) rose diagram of rock joints under different static constant normal loads in the pre-peak cyclic shear tests. It can be found from Fig. 17 that the initiated locations and propagation of cracks are mainly at the shear loading directions, which are around the 90° in DFN rose diagram. As the static constant normal loads increase, the number of cracks increases and the number of cracks located around 40°~70° increases, as shown in Fig. 17. Meanwhile, it can be found from Fig. 17 that the inclination angles of tensile and shear cracks with respect to the horizontal direction also increases as the static constant normal load increases. This phenomenon indicates the failure modes of rock joints transform from the climbing shear failure mode to the gnawing shear failure mode.

Fig. 18 shows the effect of static constant normal loads on the shear strengths and shear displacements of the rock joints with initial waviness angle of 30° subjected to the pre-peak cyclic shear loading amplitude of 50% after 500 shear cycles in the pre-peak cyclic shear tests. It can be found from Fig. 18(a) that the peak shear strength and residual shear strength increase as the static constant normal load increases, which illustrates that the increase of static normal loads leads to the increase of shear resistance induced by the increase of contact areas between rock joints. In addition, the shear displacements before the pre-peak shear cycle with amplitude of 50% decrease as the static constant normal loads increase, as shown in Fig. 18(b). Meanwhile, it can be observed from Fig. 18(b) that the shear displacement after 500 pre-peak shear cycles also decreases with increasing the static constant normal loads.

Fig. 19 shows the influence of static constant normal loads on normal dilations for rock joints containing initial waviness asperity angle of 30° after 500 shear cycles with

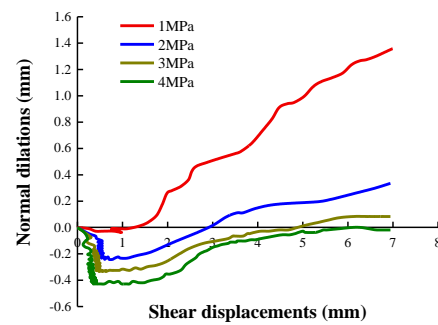


Fig. 19. Effects of static constant normal loads on normal dilations for rock joints containing initial waviness asperity angle of 30° after 500 shear cycles with 50% amplitude

50% amplitude. It can be found from Fig. 19 that the normal consolidation of rock joints increases as the static constant normal loads increases when the rock joints subjected to the low number of pre-peak shear cycles. This phenomenon demonstrates that the contact area of rock joints increases as the static constant normal loads increases under low number of pre-peak shear cycles. Meanwhile, the normal dilations of rock joints decrease with increasing the static constant normal loads, as shown in Fig. 19.

5.3 Effect of initial waviness asperity angle

To investigate the effect of initial waviness asperity angle on the shear mechanical behaviors of artificial rock joints with two-order triangular-shaped asperities, five numerical rock joints with different initial waviness asperity angle under static constant normal load of 2.0 MPa and pre-peak cyclic shear loading amplitude of 50% are numerical simulated in the bond particle numerical simulations. The initial waviness asperity angles for the five numerical rock joints are set as 5°, 15°, 30°, 45° and 60°, respectively.

Fig. 20 shows the failure patterns of five different rock joints with two-order triangular-shaped asperities under static constant normal load of 2.0 MPa and pre-peak cyclic shear loading amplitude of 50% after 500 shear cycles. It can be observed from Fig. 20(a) that the tensile cracks are

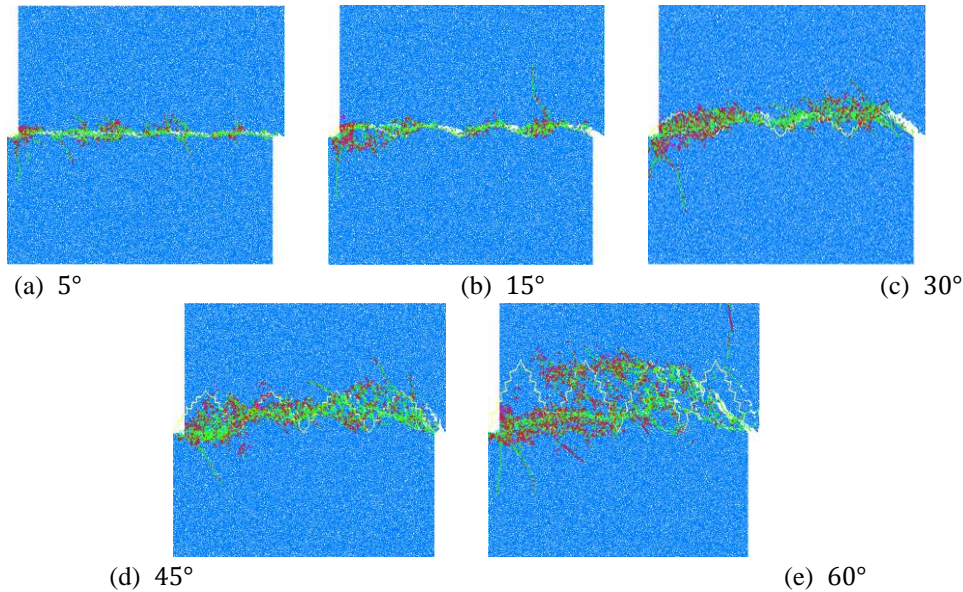


Fig. 20. Ultimate shear failure modes of rock joints with different initial waviness asperity angles after 500 shear cycles in the pre-peak cyclic shear tests

initiated and tensile crack coalescence occurs at the subordinate asperities when the initial waviness asperity angle equates to 5° . Meanwhile, a few of shear and tensile cracks initiated at the subordinate asperities propagate toward the upper and lower rock blocks as shown in Fig. 19(a). As the number of shear cracks initiated at the subordinate asperities increases with increasing the initial waviness asperity angle. For the initial waviness asperity angle of 15° , it can be found from Fig. 20(b) that not only the tensile crack coalescence occurs, but also the shear crack coalescence happens at the subordinated asperities. Meanwhile, both shear and tensile cracks initiated at the subordinate asperities propagate towards the upper and lower rock blocks, as shown in Fig. 20(b). For the initial waviness asperity angle of 30° , the combined crack coalescence of shear and tensile cracks occurs at the both primary and subordinate asperities, as shown in Fig. 20(c). For the initial waviness asperity angles of 45° and 60° , the numbers of tensile and shear cracks initiated at the subordinate asperities decreases, as shown in Fig. 20(d) and Fig. 20(e). Meanwhile, it can be found from Fig. 20(d) and Fig. 20(e) that the shear crack coalescence, tensile crack coalescence and mixed tensile-shear crack coalescence mainly occur at the primary asperities when the initial waviness asperity angles are relative high, such as 45° and 60° . Numerical results indicate that the degradations of rock joints transform from the subordinate asperity degradation to the primary asperity degradation as the initial waviness asperity angle increases. The failure types of rock joints transform tensile crack coalescence to the mixed tensile-shear crack coalescence with increasing the initial waviness asperity angle in the pre-peak cyclic shear tests.

6. Conclusions

In this study, experimental and numerical approaches are applied to investigate the pre-peak cyclic shear

mechanism of artificial rock joints. The effects of cyclic shear loading amplitude, static constant normal loads and initial waviness asperity angles on the pre-peak cyclic shear failure behaviors of triangular-shaped rock joints in direct shear tests are investigated. Some role can be concluded as follows:

- In the pre-peak cyclic shear tests, when the shear failure mode transforms from climbing shear failure mode to gnawing shear failure mode in the pre-peak cyclic shear tests, degradation of the primary and subordinate asperities changes from the shear fatigue abrasions to shear fatigue fracture.
- The shear fatigue abrasions at subordinate asperities in rock joints under low number of pre-peak shear cycles lead to the increases of contact areas between rock joints, which results in the increase of shear strength. Moreover, the shear fatigue fracture at both primary and subordinate asperities in rock joints leads to the decrease of shear strength.
- The climbing shear failure mode of artificial rock joints is mainly dominated by the tensile microscopic cracks, which belongs to the tensile failure type. The combine climbing-gnawing shear failure mode of artificial rock joints is mainly controlled by coalescences of shear cracks at both the primary and subordinate asperities, which belongs to the combined shear failure type. The gnawing shear failure mode of artificial rock joints is mainly controlled by coalescences of tensile cracks and shear cracks at both the primary and subordinate asperities, which belongs to the combined tensile-shear failure type.
- The number of microscopic cracks increases as the pre-peak cyclic shear loading amplitude increases during the pre-peak shear cyclic tests.
- The degradations of rock joints transform from the subordinate asperity degradation to the primary asperity degradation as the initial waviness asperity angle increases. The failure types of rock joints transform tensile crack

coalescence to the mixed tensile-shear crack coalescence with increasing the initial waviness asperity angle in the pre-peak cyclic shear tests.

Acknowledgment

This work is financially supported by the National Natural Science Foundation of China (Grant No. 41772319).

References

- Amiri, F., Anitescu, C., Arroyo, M., Bordas, S. and Rabczuk, T. (2014), "XFEM interpolants, a seamless bridge between XFEM and enriched meshless methods", *Comput. Mech.*, **53**(1), 45-57.
- Areias, P., Rabczuk, T. and Dias-da Costa, D. (2013), "Element-wise fracture algorithm based on rotation of edges", *Eng. Fract. Mech.*, **110**, 113-137.
- Areias, P. and Rabczuk, T. (2017), "Steiner-point free edge cutting of tetrahedral meshes with applications in fracture", *Finite Elem. Anal. Des.*, **132**, 27-41.
- Asadi, M., Rasouli, V. and Barla, G. (2012), "A bonded particle model simulation of shear strength and asperity degradation for rough rock fractures", *Rock Mech. Rock Eng.*, **45**(5), 649-675.
- Asadi, M.S., Rasouli, V. and Barla, G. (2013), "A laboratory shear cell used for simulation of shear strength and asperity degradation of rough rock fractures", *Rock Mech. Rock Eng.*, **46**(4), 683-699.
- Bagde, M.N. and Petroš, V. (2005), "Fatigue properties of intact sandstone samples subjected to dynamic uniaxial cyclical loading", *Int. J. Rock Mech. Min. Sci.*, **42**(2), 237-250.
- Bahaaddini, M., Sharrock, G. and Hebblewhite, B.K. (2013), "Numerical direct shear tests to model the shear behaviour of rock joints", *Comput. Geotech.*, **51**, 101-115.
- Bahaaddini, M., Hagan, P.C., Mitra, R. and Hebblewhite, B.K. (2014) "Scale effect on the shear behaviour of rock joints based on a numerical study", *Eng. Geol.*, **181**, 212-223.
- Bahaaddini, M., Hagan, P.C., Mitra, R. and Khosravi, M.H. (2016), "Experimental and numerical study of asperity degradation in the direct shear test", *Eng. Geol.*, **204**, 41-52.
- Bandis, S.C., Lumsden, A.C. and Barton, N.R. (1981), "Experimental studies of scale effects on the shear behaviour of rock joints", *Int. J. Rock Mech. Min. Sci. Geomech. Abstr.*, **18**(1), 1-21.
- Bandis, S.C., Lumsden, A.C. and Barton, N.R. (1983), "Fundamentals of rock joint deformation", *Int. J. Rock Mech. Min. Sci. Geomech. Abstr.*, **20**(6), 249-268.
- Barton, N. (1973), "Review of a new shear-strength criterion for rock joints", *Eng. Geol.*, **7**(4), 287-332.
- Barton, N. (1976), "The shear strength of rock and rock joints", *Int. J. Rock Mech. Min. Sci. Geomech. Abstr.*, **19**(9), 255-279.
- Barton, N. and Choubey, V. (1977), "The shear strength of rock joints in theory and practice", *Rock Mech.*, **10**(1-2), 1-54.
- Belem, T., Souley, M. and Homand, F. (2007), "Modeling surface roughness degradation of rock joint wall during direct and cyclic shearing", *Acta Geotech.*, **2**(4), 227-248.
- Benmokrane, B., Mouchaorab, K.S. and Ballivy, G. (1994), "Laboratory investigation of shaft resistance of rock-socketed piers using the constant normal stiffness direct shear test", *Can. Geotech. J.*, **31**(3), 407-419.
- Cai, X., Zhou, Z., Liu, K., Du, X. and Zhang, H. (2019), "Water-weakening effects on the mechanical behavior of different rock types: phenomena and mechanisms", *Appl. Sci.*, **9**(20), 4450.
- Cao, R.H., Cao, P., Lin, H., Pu, C. and Ke, O. (2016), "Mechanical behavior of brittle rock-like specimens with pre-existing fissures under uniaxial loading: experimental studies and particle mechanics approach", *Rock Mech. Rock Eng.*, **49**(3), 763-783.
- Cao, R.H., Cao, P., Lin, H., Ma, G. and Chen, Y. (2018), "Failure characteristics of intermittent fissures under a compressive-shear test: Experimental and numerical analyses", *Theor. Appl. Fract. Mech.*, **96**, 740-757.
- Cho, N., Martin, C.D. and Sego, D.C. (2007), "A clumped particle model for rock", *Int. J. Rock Mech. Min. Sci.*, **44**(7), 997-1010.
- Dang, W., Konietzky, H. and Frühwirt, T. (2016), "Direct shear behavior of a plane joint under dynamic normal load (DNL) conditions", *Eng. Geol.*, **213**, 133-141.
- Dang, W.G., Konietzky, H. and Chang, L. (2018), "Velocity-frequency-amplitude-dependent frictional resistance of planar joints under dynamic normal load (DNL) conditions", *Tunnel Undergr. Space Technol.*, **79**, 27-34.
- Dang, W., Konietzky, H., Frühwirt, T. and Herbst, M. (2019), "Cyclic Frictional Responses of Planar Joints Under Cyclic Normal Load Conditions: Laboratory Tests and Numerical Simulations", *Rock Mech. Rock Eng.* doi:10.1007/s00603-019-01910-9.
- Eshiet, K. and Sheng, Y. (2014), "Investigation of geomechanical responses of reservoirs induced by carbon dioxide storage", *Environ. Earth. Sci.*, **71**(9), 3999-4020.
- Eshiet, K. and Shen, Y. (2017), "The role of rock joint frictional strength in the containment of fracture propagation", *Acta Geotech.*, **12**(4), 897-920.
- Fakhimi, A. (2004), "Application of slightly overlapped circular particles assembly in numerical simulation of rocks with high friction angles", *Eng. Geol.*, **74**(1-2), 129-138.
- Fathi, A., Moradian, Z., Rivard, P. and Ballivy, G. (2016), "Shear mechanism of rock joints under pre-peak cyclic loading condition", *Int. J. Rock Mech. Min. Sci.*, **83**, 197-210.
- Ferrero, A.M., Migliazza, M. and Tebaldi, G. (2010), "Development of a new experimental apparatus for the study of the mechanical behavior of a rock discontinuity under direct and cyclic loads", *Rock Mech. Rock Eng.*, **43**(6), 685-695.
- Gu, D.M., Huang, D., Yang, W.D., Zhu, J.L. and Fu, G.Y. (2017), "Understanding the triggering mechanism and possible kinematic evolution of a reactivated landslide in the Three Gorges Reservoir", *Landslides*, **14**(6), 2073-2087.
- Haeri, H., Sarfarazi, V., Zhu, Z., Hedayat, A., Nezamabadi, M.F. and Karbala M. (2018a), "Simulation of crack initiation and propagation in three point bending test using PFC2D", *Struct. Eng. Mech.*, **66**(4), 453-463.
- Haeri, H., Sarfarazi, V., Zhu, Z. and Lazemi, H.A. (2018b), "Investigation of the effects of particle size and model scale on the UCS and shear strength of concrete using PFC2D", *Struct. Eng. Mech.*, **67**(5), 505-516.
- Haeri, H., Sarfarazi, V., Zhu, Z. and Marji, M.F. (2018c), "Simulation of the tensile failure behaviour of transversally bedding layers using PFC2D", *Struct. Eng. Mech.*, **67**(5), 493-504.
- Haeri, H., Sarfarazi, V. and Zhu, Z. (2018d), "PFC3D simulation of the effect of particle size on the single edge-notched rectangle bar in bending test", *Struct. Eng. Mech.*, **68**(4), 497-505.
- Haeri, H., Sarfarazi, V. and Zhu, Z. (2018e), "Numerical simulation of the effect of bedding layer geometrical properties on the punch shear test using PFC3D", *Struct. Eng. Mech.*, **68**(4), 507-517.
- Huang, T.H., Chang, C.S. and Chao, C.Y. (2002), "Experimental and mathematical modeling for fracture of rock joint with regular asperities", *Eng. Fract. Mech.*, **69**(17), 1977-1996.
- Huang, D., Cen, D., Ma, G. and Huang, R. (2015), "Step-path failure of rock slopes with intermittent joints", *Landslides*, **12**(5), 911-926.
- Huang, Y.H., Yang, S.Q. and Zhao, J. (2016), "Three-Dimensional Numerical Simulation on Triaxial Failure Mechanical Behavior

- of Rock-Like Specimen Containing Two Unparallel Fissures”, *Rock Mech. Rock Eng.*, **49**(12), 4711-4729.
- Huang, Y.H., Yang, S.Q. and Zhao, J. (2017), “Strength failure behavior and crack evolution mechanism of granite containing pre-existing non-coplanar holes: experimental study and particle flow modeling”, *Comput. Geotech.*, **88**, 182-198.
- Huang, Y.H., Yang, S.Q. and Tian, W.L. (2019), “Crack coalescence behavior of sandstone specimen containing two pre-existing flaws under different confining pressures”, *Theor. Appl. Fract. Mech.*, **99**, 118-130.
- Huang, Y.H. and Yang, S.Q. (2019), “Mechanical and cracking behavior of granite containing two coplanar flaws under conventional triaxial compression”, *Int. J. Damage Mech.*, **28**(4), 590-610.
- Jafari, M.K., Hosseini, K.A., Pellet, F., Boulon, M. and Buzzi, O. (2003), “Evaluation of shear strength of rock joints subjected to cyclic loading”, *Soil Dyn. Earthq. Eng.*, **23**(7), 619-630.
- Jafari, M.K., Pellet, F., Boulon, M. and Amini Hosseini, K. (2004), “Experimental study of mechanical behavior of rock joints under cyclic loading”, *Rock Mech. Rock Eng.*, **37**(1), 3-23.
- Jiang, Y., Xiao, J., Tanabashi, Y. and Mizokami, T. (2004) “Development of an automated servo-controlled direct shear apparatus applying a constant normal stiffness condition”, *Int. J. Rock Mech. Min. Sci.*, **41**(2), 275-286.
- Johnston, I.W., Lam, T.S. and Williams, A.F. (1987), “Constant normal stiffness direct shear testing for socketed pile design in weak rock”, *Geotechnique* **37**(1), 83-89.
- Kou, M.M., Lian, Y.J. and Wang, Y.T. (2019a), “Numerical investigations on crack propagation and crack branching in brittle solids under dynamic loading using bond-particle mode”, *Eng. Fract. Mech.*, **212**, 41-56.
- Kou, M., Liu, X., Tang, S. and Wang, Y. (2019b), “3-D X-ray computed tomography on failure characteristics of rock-like materials under coupled hydro-mechanical loading”, *Theor. Appl. Fract. Mech.*, **104**, 102396.
- Kou, M., Han, D., Xiao, C. and Wang, Y. (2019c), “Dynamic fracture instability in brittle materials: Insights from DEM simulations”, *Struct. Eng. Mech.*, **71**(1), 65-75.
- Kou, M., Liu, X., and Wang, Y. (2020), “Study on rock fracture behavior under hydromechanical loading by 3-D digital reconstruction. Structural Engineering and Mechanics”, *Struct. Eng. Mech.*, **74**(2), 1-14.
- Lee, H.S., Park, Y.J., Cho, T.F. and You, K.H. (2001), “Influence of asperity degradation on the mechanical behavior of rough rock joints under cyclic shear loading”, *Int. J. Rock Mech. Min. Sci.*, **38**(7), 967-980.
- Li, X. and Chen, J. (2017). “An extended cohesive damage model for simulating arbitrary damage propagation in engineering materials”, *Comput. Methods Appl. Mech. Engrg.*, **315**, 744-759.
- Li, X., Gao, W. and Liu, W. (2019), “A mesh objective continuum damage model for quasi-brittle crack modelling and finite element implementation”, *Int. J. Damage Mech.*, **28**(9), 1299-1322.
- Liu, Y., Dai, F., Zhao, T. and Xu, N.W. (2017), “Numerical investigation of the dynamic properties of intermittent jointed rock models subjected to cyclic uniaxial compression”, *Rock Mech. Rock Eng.*, **50**(1), 89-112.
- Mehrian, S. Z., Amrei, S. R., Maniat, M. and Nowruzpour Mehrian, S.M. (2016), “Structural health monitoring using optimising algorithms based on flexibility matrix approach and combination of natural frequencies and mode shapes”, *Int. J. Struct. Eng.*, **7**(4), 398-411.
- Meng, F., Zhou, H., Li, S., Zhang, C., Wang, Z., Kong, L. and Zhang, L. (2016), “Shear behaviour and acoustic emission characteristics of different joints under various stress levels”, *Rock Mech. Rock Eng.*, **49**(12), 4919-4928.
- Meng, F., Zhou, H., Wang, Z., Zhang, C., Li, S., Zhang, L. and Kong, L. (2018a), “Characteristics of asperity damage and its influence on the shear behavior of granite joints”, *Rock Mech. Rock Eng.*, **51**(2), 429-449.
- Meng, F., Wong, L.N.Y., Zhou, H. and Wang, Z. (2018b), “Comparative study on dynamic shear behavior and failure mechanism of two types of granite joint”, *Eng. Geol.*, **245**, 356-369.
- Mirzaghorbanali, A., Nemcik, J. and Aziz, N. (2014a), “Effects of cyclic loading on the shear behavior of infilled rock joints under constant normal stiffness conditions”, *Rock Mech. Rock Eng.*, **47**(4), 1373-1391.
- Mirzaghorbanali, A., Nemcik, J. and Aziz, N. (2014b), “Effect of shear rate on cyclic loading shear behavior of rock joints under constant normal stiffness conditions”, *Rock Mech. Rock Eng.*, **47**(5), 1931-1938.
- Mohammed, T.J., Bakar, B.H.A. and Bunnori, A.B. (2015), “Strengthening of reinforced concrete beams subjected to torsion with UHPFC composites”, *Struct. Eng. Mech.*, **56**(1), 123-136.
- Moradian, Z.A., Ballivy, G., Rivard, P., Gravel, C. and Rousseau, B. (2010), “Evaluating damage during shear tests of rock joints using acoustic emission”, *Int. J. Rock Mech. Min. Sci.*, **47**(4), 590-598.
- Moradian, Z.A., Ballivy, G. and Rivard, P. (2012), “Correlating acoustic emission sources with damaged zones during direct shear test of rock joints”, *Can. Geotech. J.*, **49**(6), 710-718.
- Moës, N. and Belytschko, T. (2002), “Extended finite element method for cohesive crack growth”, *Eng. Fract. Mech.*, **69**(7), 813-833.
- Nanthakumar, S., Lahmer, T., Zhuang, X., Zi, G. and Rabczuk, T. (2016), “Detection of material interfaces using a regularized level set method in piezoelectric structures”, *Inverse Probl. Sci. Eng.*, **24**(1), 153-176.
- Nowruzpour, M., Sarkar, S., Reddy, J.N. and Roy, D. (2019), “A derivative-free upscaled theory for analysis of defects”, *J. Mech. Phys. Solids*, **122**, 89-501.
- Nowruzpour, M. and Reddy, J.N. (2018), “Unification of local and nonlocal models within a stable integral formulation for analysis of defects”, *Int. J. Eng. Sci.*, **132**, 45-59.
- Nowruzpour Mehrian, S.M., Roozbahani, M.M. and Mehrian S.Z., Fathi, A. (2013), “Comprehensive Investigation in Buckling and Free Vibration of Laminate Composite cylindrical Shell”, *J. Bas. Appl. Sci. Res.*, **3**(5), 195-205.
- Ooi, L.H. and Carter, J.P. (1987), “A constant normal stiffness direct shear device for static and cyclic loading”, *ASTM Geotech. Test J.*, **10**(1), 3-12.
- Park, J.W. and Song, J.J. (2009), “Numerical simulation of a direct shear test on a rock joint using a bonded-particle model”, *Int. J. Rock Mech. Min. Sci.*, **46**(8), 1315-1328.
- Potyondy, D.O. and Cundall, P.A. (1998), “Modeling notch-formation mechanisms in the URL mine-by test tunnel using bonded assemblies of circular particles”, *Int. J. Rock Mech. Min. Sci. Geomech. Abstr.*, **35**(4-5), 510-511.
- Potyondy D.O. and Cundall, P.A. (2004), “A bonded-particle model for rock”, *Int. J. Rock Mech. Min. Sci.*, **41**(8), 1329-1364.
- PFC2D (2004), “Particle Flow Code in 2 Dimensions-Version 3.1”, Itasca Cons Group, Minneapolis.
- Sarfarazi, V. and Haeri, H. (2018), “Three-dimensional numerical modeling of effect of bedding layer on the tensile failure behavior in hollow disc models using Particle Flow Code (PFC3D)”, *Struct. Eng. Mech.*, **68**(5), 537-547.
- Seidel, J.P. and Haberfield, C.M. (2002), “A theoretical model for rock joints subjected to constant normal stiffness direct shear”, *Int. J. Rock Mech. Min. Sci.*, **39**(5), 539-553.
- Song, Z., Konietzky, H. and Herbst, M. (2019), “Bonded-particle model-based simulation of artificial rock subjected to cyclic loading”, *Acta Geotech.*, **14**(4), 955-971.
- Song, Z., Frühwirth, T. and Konietzky, H. (2020), “Inhomogeneous

- mechanical behaviour of concrete subjected to monotonic and cyclic loading”, *Int J Fatigue*, **132**, 105383.
- Wang, Y., Zhou, X. and Xu, X. (2016), “Numerical simulation of propagation and coalescence of flaws in rock materials under compressive loads using the extended non-ordinary state-based peridynamics”, *Eng. Fract. Mech.*, **163**, 248-273.
- Wang, Y., Zhou, X. and Shou, Y. (2017), “The modeling of crack propagation and coalescence in rocks under uniaxial compression using the novel conjugated bond-based peridynamics”, *Int. J. Mech. Sci.*, **128-129**, 614-643.
- Wang, Y., Zhou, X., Wang, Y. and Shou, Y. (2018a), “A 3-D conjugated bond-pair-based peridynamic formulation for initiation and propagation of cracks in brittle solids”, *Int. J. Solids Struct.*, **134**, 89-115.
- Wang, Y., Zhou, X. and Kou, M. (2018b), “Peridynamic investigation on thermal fracturing behavior of ceramic nuclear fuel pellets under power cycles”, *Ceram. Int.*, **44**(10), 11512-11542.
- Wang, Y., Zhou, X. and Kou, M. (2018c), “Numerical studies on thermal shock crack branching instability in brittle solids”, *Eng. Fract. Mech.*, **204**, 157-184.
- Wang, Y., Zhou, X. and Kou, M. (2018d), “A coupled thermo-mechanical bond-based peridynamics for simulating thermal cracking in rocks”, *Int. J. Fract.*, **211**(1-2), 13-42
- Wang, Y., Zhou, X. and Kou, M. (2019a), “Three-dimensional numerical study on the failure characteristics of intermittent fissures under compressive-shear loads”, *Acta Geotech.*, **14**(4), 1161-1193
- Wang, Y., Zhou, X. and Kou, M. (2019b), “An improved coupled thermo-mechanic bond-based peridynamic model for cracking behaviors in brittle solids subjected to thermal shocks.”, *Eur. J. Mech. A-Solid*, **73**, 282-305
- Wang, L., Xu, J., Wang, J. and Karihaloo, B.L. (2019c), “A mechanism-based spatiotemporal non-local constitutive formulation -for elastodynamics of composites”, *Mech. Mater.*, **128**, 105-116.
- Wang, L., Xu, J. and Wang, J. (2019d), “Elastodynamics of Linearized Isotropic State-Based Peridynamic Media”, *J. Elast.*, **137**, 157-176.
- Xie, Y., Cao, P., Liu, J. and Dong, L. (2016), “Influence of crack surface friction on crack initiation and propagation: A numerical investigation based on extended finite element method”, *Comput. Geotech.*, **74**, 1-14
- Yang, Z.Y., Di, C.C. and Yen, K.C. (2001), “The effect of asperity order on the roughness of rock joints”, *Int. J. Rock Mech. Min. Sci.*, **38**(5), 745-752
- Yang, D., Zhang, D., Niu, S., Dang, Y., Feng, W. and Ge, S. (2018) “Experiment and study on mechanical property of sandstone post-peak under the cyclic loading and unloading”, *Geotech. Geol. Eng.*, **36**(3), 1609-1620.
- Zhang, X.P. and Wong, L.N.Y. (2012), “Cracking processes in rock-like material containing a single flaw under uniaxial compression: a numerical study based on parallel bonded-particle model approach”, *Rock Mech. Rock Eng.*, **45**(5), 711-737.
- Zheng, B. and Qi, S. (2012), “A new index to describe joint roughness coefficient (JRC) under cyclic shear”, *Eng. Geol.*, **212**, 72-85.
- Zhou, H., Meng, F., Zhang, C., Hu, D., Lu, J. and Xu, R (2016) “Investigation of the acoustic emission characteristics of artificial saw-tooth joints under shearing condition”, *Acta Geotech.*, **11**(4), 925-939.
- Zhou, X.P. and Wang, Y.T. (2016) “Numerical simulation of crack propagation and coalescence in pre-cracked rock-like Brazilian disks using the non-ordinary state-based peridynamics”, *Int. J. Rock Mech. Min. Sci.*, **89**, 235-249.
- Zhou, X., Wang, Y., Shou, Y. and Kou, M. (2018), “A novel conjugated bond linear elastic model in bond-based peridynamics for fracture problems under dynamic loads”, *Eng. Fract. Mech.*, **188**, 151-183.
- Zhou, Z., Cai, X., Li, X., Cao, W. and Du, X. (2019a), “Dynamic Response and Energy Evolution of Sandstone Under Coupled Static-Dynamic Compression: Insights from Experimental Study into Deep Rock Engineering Applications”, *Rock Mech. Rock Eng.*, 1-27.
- Zhou, Z., Wang, H., Cai, X., Chen, L., Yude, E. and Chen, R. (2019b), “Damage Evolution and Failure Behavior of Post-Mainshock Damaged Rocks under Aftershock Effects”, *Energies*, **12**(23), 4429.
- Zhou, X.P., Wang, Y.T., Zhang, J.Z. and Kou, M.M. (2019c), “Fracturing behavior study of three-flawed specimens by uniaxial compression and 3D digital image correlation: sensitivity to brittleness”, *Rock Mech. Rock Eng.*, **52**(3), 691-718.

CC